An engineered planar plasmonic reflector for polaritonic mode confinement

Shima Rajabali,[*,†] Josefine Enkner,[†] Erika Cortese,[‡] Mattias Beck,[†] Simone De Liberato,[*,‡] Jérôme Faist,[†] and Giacomo Scalari[*,†]

†*Institute of Quantum Electronics, ETH Zürich, 8093 Zürich, Switzerland*

‡*School of Physics and Astronomy, University of Southampton, Southampton, SO17 1BJ, United Kingdom*

E-mail: shimar@phys.ethz.ch; s.de-liberato@soton.ac.uk; scalari@phys.ethz.ch

Abstract

It was recently demonstrated that, in deep subwavelength gap resonators coupled to two-dimensional electron gases, propagating plasmons can lead to energy leakage and prevent the formation of polaritonic resonances. This process, akin to Landau damping, limits the achievable field confinement and thus the value of light-matter coupling strength. In this work, we show how plasmonic reflectors can be used to create an artificial energy stopband in the plasmon dispersion, confining them and enabling the recovery of the polaritonic resonances. Using this approach we demonstrate a normalized light-matter coupling ratio of $\frac{\Omega_R}{\omega_0} = 0.36$ employing a single doped quantum well with a resonator's gap size of 250 nm equivalent to $\lambda/3000$ in vacuum, a geometry in which the polaritonic resonances would not be observable in the absence of the plasmonic reflectors.

Introduction

The terahertz (THz) range combines material systems with large optical dipoles with extremely subwavelength resonant cavities obtained by exploiting metals in a lumped-circuit approach.[1,2] It is thus especially suited for the study of ultrastrong light-matter coupling phenomena,[3,4] in which the light-matter coupling, quantified by the vacuum Rabi frequency Ω_R becomes of the order of the bare frequency of the resonant light and matter modes ω_0. The Landau polariton platform,[5,6] in which a photonic resonator is coupled to a two-dimensional electron gas (2DEG) under applied magnetic field, has proven especially successful in obtaining values of the normalized coupling constant larger than one ($\frac{\Omega_R}{\omega_0} > 1$, where Ω_R is the resonant vacuum Rabi frequency and ω_0 the cyclotron frequency).[7] and extremely high cooperativity.[8,9] These features made Landau polaritons an ideal testbed to explore many strong-coupling phenomena, as the influence of enhanced vacuum fields on the DC magnetotransport both in the linear[10] and the integer Quantum Hall regimes,[11] and the dynamical manipulation of the real-space profile of the polaritonic electromagnetic field.[12] Several demonstrations of few-electron systems have also been realized in Landau polariton platforms.[1,13,14]

Reducing the modal volume of the electromagnetic resonator allows both to increase the strength of the light-matter coupling and to reduce the number of involved electrons,[15] thus approaching the non-linear polaritonic regime. In standard nanophotonic platforms, both metallic[16] and dielectric,[17] this strategy is known to break down for resonator features small enough to excite propagative charge waves. In this case the standard local description of light-matter coupling fails and more accurate nonlocal approaches have to be used.[18,19]

Our recent work[20] demonstrated the existence of a related effect in Landau polaritons due to the nonlocal excitation of propagative two-dimensional (2D) plasmons, limiting the possibility of arbitrarily increasing the light-matter coupling by reducing the modal volume of the photonic resonator. In the aforementioned Landau-polariton paper, the magnetoplasmons which are collective inter-Landau level excitations are (ultra)strongly coupled to the elec-

tromagnetic field confined in the gap of metamaterial complementary split-ring resonators (cSRR). We observed the progressive broadening and amplitude reduction of the upper polariton (UP) mode and the partial disappearance of the lower polariton (LP) branch by reducing the gap of the coupled cSRRs below a critical length of the order of hundreds of nanometers. This length is three orders of magnitude larger than the lengthscale relevant for nonlocality in metals[16] and one order of magnitude larger than the one relevant for nonlocality in dielectrics.[17] The observed phenomena cannot thus be due to the nonlocal response of the cSRR. We discovered that the explanation lies instead in the nonlocal response of the electron gas coupled to the cSRR to form the polaritons, and it is caused by Landau damping due to the continuum of high-momenta propagative 2D magnetoplasmons excited by strongly subwavelength fields confinement. These propagating modes act as loss channels and ultimately limit the achievable strength of the light-matter coupling, which depends on the overlap between the photonic and the electronic eigenmnodes. As a result, polaritonic modes can broaden or disappear, and the system enters a new regime of discrete-to-continuum strong coupling.[21–23] In this work we show how, by creating engineered plasmonic reflectors around the gap of the resonator, thus creating an effective plasmonic resonator, we can again confine these propagating waves and retrieve well-defined polariton branches.

Methods

Reflector design

In order to confine the broadened polaritonic mode whose energy is leaking out as a result of polaritonic nonlocal effects, we aim to introduce a plasmonic bandgap structure: two planar reflectors in the magnetoplasmon propagation path, similar to plasmonic Bragg reflectors,[24,25] confining the 2D plasmons between them. To implement such a planar reflectors for the magnetoplasmon waves, we need to introduce a spatial modulation of the plasmonic

dispersion, akin to a modulation of the refractive index in optical Bragg reflectors. One simple method is to introduce a modulation in the carrier density of the 2DEG by structuring the 90 nm-thick gallium arsenide (GaAs) cap layer on top of a quantum well channel with nominal doping $\rho_{2DEG} = 3.2 \times 10^{11}\text{cm}^{-2}$, as illustrated in Fig. 1. This structure, made

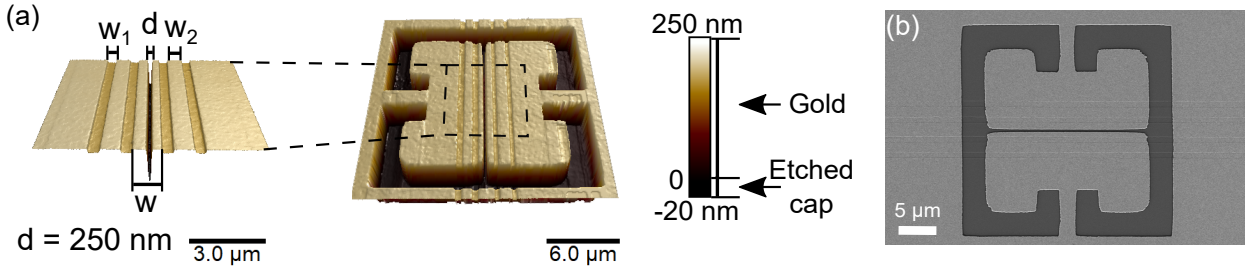

Figure 1: **The scheme of the plasmonic reflector design.** (a) The 3D image, taken by atomic force microscopy, of the cSRR with a gap size of $d = 250\,\text{nm}$ on top a plasmonic reflector (the periodic $h = 20\,\text{nm}$ trenches on the top of the 2DEG). The parameters d, w_1, w_2, and w are 0.25, 1, 1, and 1.5 µm, respectively. (b) A scanning electron microscopy image of the same structure shown in panel (a).

by etching shallow $h = 20\,\text{nm}$ trenches can define a stop-band in the transmission spectrum of the wave propagating across the 2DEG plane.[24,25] By introducing a defect of width $w = 1.5\,\mu\text{m}$ at the center of this periodic (2 periods) structure, modes can be also defined inside the stop-band.

Such a periodic structure with a central defect around the sub-micron gap of the cSRR should allow, by reconfining the 2D plasmons, to retrieve the contrast in the amplitude and enhance the lifetime of the polaritonic modes, effectively decoupling them from the lossy continuum of propagating plasmonic modes. The three dimensional image of the fabricated resonator measured by atomic force microscopy is also exhibited in Fig. 1a, indicating the important design parameters such as the resonator's gap (d), the central defect's width (w), and the width of the periodic structure of the reflector (w_1 and w_2).

Sample fabrication

To fabricate the plasmonic reflector, the trenches were initially defined using a direct laser writing lithography with Heidelberg DWL66+. The trenches were etched by a highly diluted etching solution (*slow etchant solution*: H_2O, 1 : 3). The slow etchant solution itself was made of ($H_2SO_4 : H_2O_2 : H_2O$, 1 : 8 : 60) with an etch rate of $\sim 9\,\mathrm{nm/s}$ for semi-insulating GaAs. The diluted solution had an etch rate of $\sim 3\,\mathrm{nm/s}$ for semi-insulating GaAs. Reducing the etch rate was done to increase the etching time and its accuracy, to be able to etch only a few tens of nanometers. The etch rates were evaluated by a Dektak surface step profiler (with a 5 µm radius tip) and a scanning electron microscopy. After an aligning step, the cSRRs were fabricated on top of the etched trenches with electron beam lithography using a bilayer resist process with 450 nm 495K-PMMA-A4 and 90 nm Dow Corning XR-1541-006 electron beam negative resist. The lithography step was followed by deposition of 4 nm titanium and 200 nm of gold and a lift-off process. After a set of finite element simulation to find the right dimensions for reconfining the UP mode, a sample with a trench depth of $h = 20\,\mathrm{nm}$ was chosen and fabricated. Figure 1b shows a scanning electron microscopy image of the etched trenches in the 2DEG with a cSRR on top. The resonators were aligned and written on the etched substrate using electron-beam lithography.

Spectroscopic measurements

The measurements are conducted in a THz time-domain spectroscopy (TDS) setup at cryogenic temperature T = 2.7 K as a function of an external out-of-plane magnetic field swept between 0 and 4 T. In the THz-TDS setup, a pair of off-axis parabolic mirrors first are used to collimate and focus the incident THz beam from a photoconductive switch[26] on the sample. Then, through another pair of off-axis parabolic mirrors, the transmitted signal from the sample is collected, collimated, and focused on a zinc telluride (ZnTe) crystal. Ultimately, the THz signal is detected using an electro-optic detection scheme.[27] Detailed information about the THz-TDS setup is available in Ref.[28]

Results and Discussion

Experimental results

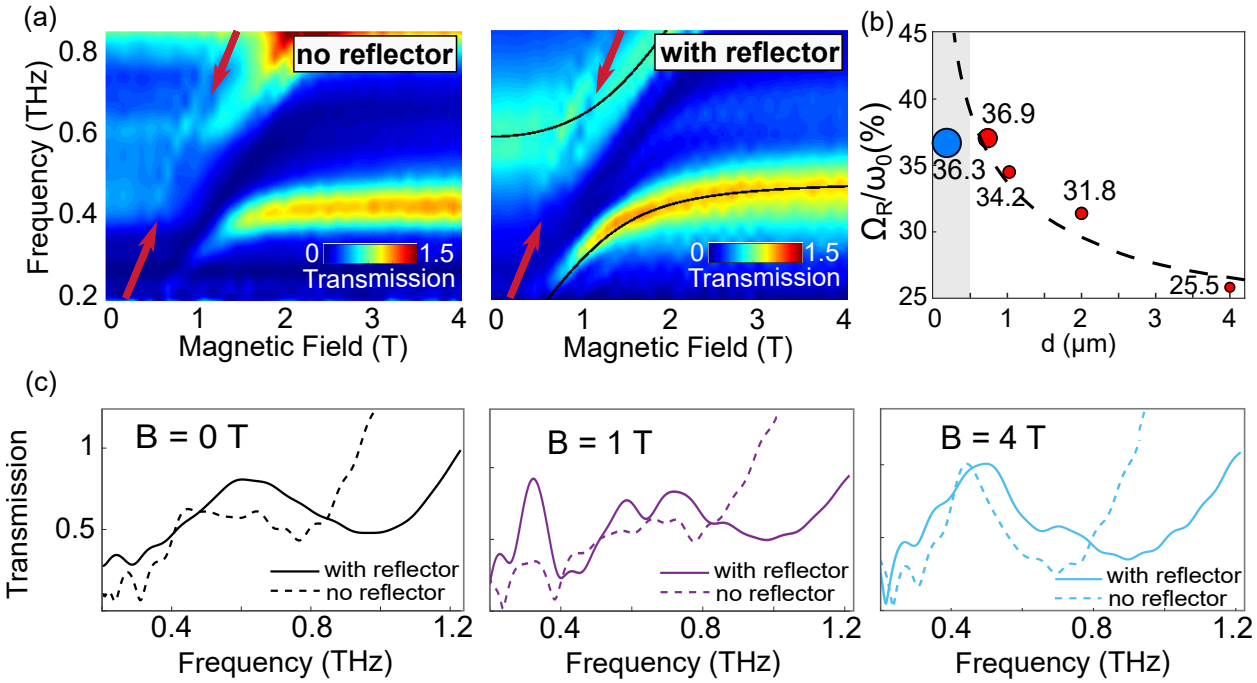

Figure 2: **Recovering polaritons using plasmonic reflectors.** (a) The measured transmission of the coupled cSRR to inter-Landau level transitions in a 2DEG without and with the plasmonic reflector (with $h = 20\,\text{nm}$ etching depth). The data without the reflector illustrate the nonlocal effects (broadening of the UP mode and disappearance of the LP mode for a finite value of the magnetic field), while the data with the reflector show normal polaritonic features, demonstrating the confinement of the 2D plasmons. The polariton branches from the measurement of the sample with reflector are fitted by a Hopfield model (black solid lines), extracting a normalized coupling of $\frac{\Omega_R}{\omega_0} = 36.3\%$. The red arrows mark the linear dispersions at multiple of the cyclotron frequency discussed in the main text. (b) Normalized coupling versus the gap of the cSRR d. The dashed black line indicates the predicted dependence of $\frac{\Omega_R}{\omega_0}$ on $\frac{1}{\sqrt{d}}$. The gray shading marks the region where the excessive broadening of the UP due to Landau damping does not allow a measurement of the light-matter coupling. The circle diameters are proportional to the fitting error. The results marked by red dots are taken from Ref.,[20] the blue one is the measurement performed in this paper. (c) Sections of experimental data in panel (a) at three different values of the magnetic field, $B = 0$, 1 (anti-crossing), and 4 T with (solid) and without (dashed) the plasmonic reflector.

Figure 2a shows the transmission measurement for the cSRR with $d = 250\,\text{nm}$ gap size on a plasmonic reflector with $h = 20\,\text{nm}$-deep trenches. The transmission measurement without and with the reflectors in Fig. 2a clearly shows how the reflectors allow to mitigate

the effects of nonlocality, showing well-defined LP and UP resonances extending toward zero magnetic field as predicted by a standard local Hopfield theory with a normalized coupling $\frac{\Omega_R}{\omega_0} = 36.3\%$ (black solid lines).[29] In Figure 2b we updated the plot from Ref.[20] with the new experimental point measured with the reflector. The values of $\frac{\Omega_R}{\omega_0}$ measured in our previous publications (red dots) are plotted against the value of the central gap d, with the shaded region indicating the nonlocal region in which the standard Hopfield model failed. With the blue dot we mark instead the value $\frac{\Omega_R}{\omega_0} = 36.3\%$ measured in this work. We can see how, while the values measured in Ref.[20] follow the $\frac{1}{\sqrt{d}}$ dependency theoretically predicted by the Hopfield model[29] and marked in the figure with a black dashed line, the value measured in the reflector sample is substantially smaller of what would be predicted for $d = 250$ nm and more in line with what expected for a micron-sized gap. This phenomenon can be explained by noticing that, while the fundamental electromagnetic mode of the cSRR is confined in the central gap of width $d = 250$nm, the plasmonic reflectors confine the plasmons in the central defect of width $w = 1.5\mu$m (Animated electric-field distribution are provided in Visualization 1-3). The coupling between light and matter is proportional to the integral of the overlap between the photonic and plasmonic wavefunctions[12] and the coupling strength is thus limited by the looser plasmonic confinement. For a better comparison between the polaritonic modes measured on the samples without and with the reflectors, sections of the colormaps at three different values of the magnetic field, $B = 0$, 1 (anti-crossing), and 4 T are displayed in Fig. 2c.

Note that the linear dispersions corresponding to optical transitions at multiples of the cyclotron frequency (indicated with red arrows in Fig. 2a), also reported in a previous work,[20] are unaffected by the presence of the reflector structure, appearing at the same place in both panels.

Theoretical and numerical analysis

In order to confirm our interpretation we have simulated the transmission spectra of the coupled system with and without the reflector structure as a function of the magnetic field using a finite element method. Results are shown in Fig. 3. Given the difficulty of precisely modeling the modulation of the 2DEG's density due to the partial etching of the cap layer (only 20 out of 90 nm of the cap layer are etched, ensuring the 2DEG extends over the whole structure), we simulated trenches etched both to $h = 80\,\mathrm{nm}$ and to the full $h = 90\,\mathrm{nm}$, the latter corresponding to having the gold in the cSRR directly in contact with the 2DEG and thus to a hard border for the 2D plasmon propagation. The normalized coupling fitted with the standard, local Hopfield model to the simulated data with nominal parameters are $\frac{\Omega_R}{\omega_0} = 40.5\%$ for $h = 80\,\mathrm{nm}$ and $\frac{\Omega_R}{\omega_0} = 41.9\%$ for $h = 90\,\mathrm{nm}$. The results obtained from the simulations both with and without the reflectors match the experimental ones, with the upper polariton substantially narrower in the presence of the reflector, and even more for the totally etched cap layer. The simulated electric field distribution of the upper polariton at finite magnetic fields (marked with star symbols in the top row) are also demonstrated in the bottom row of Fig. 3, showing partially/fully confinement of the excited magnetoplasma waves in the presence of the plasmonic reflector. To visually demonstrate the propagation of the plasma waves, the animated versions of field distribution plots, where the phase of the incident field is changing, are provided in Visualizations 1-3. Moreover, an additional mode starts appearing at 405 GHz at zero magnetic field in the simulation with the partially etched cap layer.

While this extra mode is only barely visible the simulation performed with the 2DEG extending below the full structure, it becomes much better defined in the simulation with a totally etched cap layer, in which also a second extra mode at 834 GHz becomes visible. To understand the nature of these modes we start writing down the dispersion for the 2D

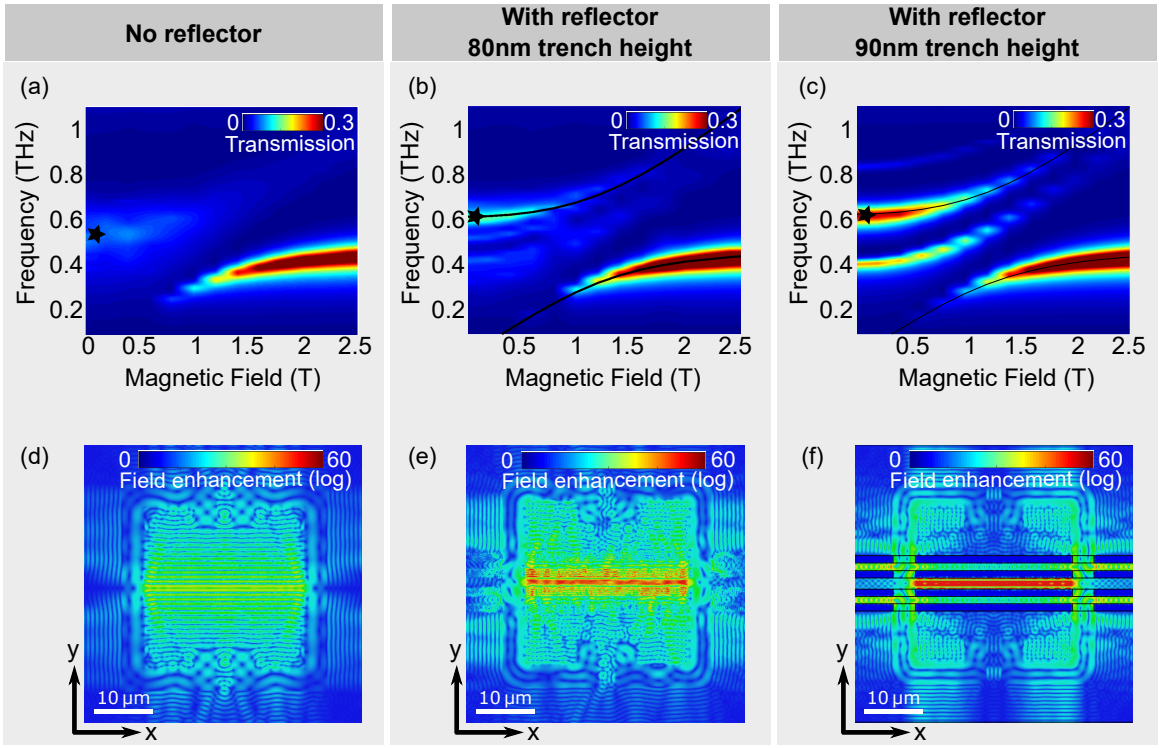

Figure 3: **Finite element simulation of the coupled structure without and with the reflector structure.** *a-c:* The simulated transmission spectra as a function of magnetic field are shown for the coupled cSRRs with a gap of $d = 250$ nm (a) without the reflector structure and with the reflector structure and a cap layer etched to (b) $h = 80$ nm and (c) $h = 90$ nm. Similar to the observed measured data in Fig. 2a, the upper polariton in the sample without the reflector is broadened (panel a). The upper polariton is substantially narrower in the spectrum of the simulated structures with the reflector (in both partially/totally etched caps). In the case of the 90 nm etched cap layer, where a hard boundary is created for the 2D plasmon propagation, three plasmonic modes starting from 405, 620, and 834 GHz at zero magnetic field appear in the transmission spectrum (panel c). The polariton branches are fitted by a Hopfield model (black solid lines), extracting a normalized coupling of $\frac{\Omega_R}{\omega_0} = 40.5\%$ (panel b) and $\frac{\Omega_R}{\omega_0} = 41.9\%$ (panel c). *d-f:* The electric field distribution of the upper polariton mode marked in the top row (black star symbol). The 2D plane is located at the plane of the 2DEG ($z = z_{2DEG}$). The plot corresponding to the coupled cSRR without the reflector (panel d) clearly demonstrates the excitation of plasmonic waves and the nonlocal effect. However, in the structures with the reflector, the plasmonic reflector confines the plasmons in the central defect of width $w = 1.5\mu$m, partially for a cap layer etched to $h = 80$ nm (panel e) and fully for the one etched to $h = 90$ nm (panel f).

plasmons for a homogeneous 2DEG, which has form

$$\omega_P(k) \;=\; \sqrt{\frac{ke^2\rho_{2DEG}}{2m^*\epsilon_0\bar{\epsilon}(k)}}, \tag{1}$$

where ρ_{2DEG} is the 2DEG density, m^* the electron effective mass, and $\bar{\epsilon}(k)$ is the background effective dielectric function, in general k-dependent, describing the screening of surrounding dielectric and/or metallic gates in the system.[30] The analytical expression for the dielectric function was derived by Chaplik[31] in his study of the optical response of plasma oscillations in 2DEG systems capped by a dielectric barrier of thickness l, both in the presence and absence of a metallic gate. By calculating the potential energy of the charges in a crystal lattice, and thus the elastic constants matrix determining their oscillation frequencies, he found, for the two different configurations, effective dielectric functions, respectively, of the form

$$\epsilon_{\mathrm{Au}}(k) = \frac{\epsilon_r}{2}\left[1+\coth\left(kl\right)\right], \tag{2}$$

and

$$\epsilon_{\mathrm{Air}}(k) = \frac{\epsilon_r}{2}\left[1+\frac{1+\epsilon_r\tanh(kl)}{\epsilon_r+\tanh(kl)}\right], \tag{3}$$

with ϵ_r the background dielectric constant of GaAs. In particular, the presence of a metallic plane in close proximity to the top of the 2DEG ($kl \ll 1$) leads the dispersion to diverge from its standard square-root-dependence and to acquire a linear acoustic behaviour

$$\lim_{kl\to 0}\omega_P(k)|_{\bar{\epsilon}=\epsilon_{\mathrm{Au}}} \;\approx\; \sqrt{\frac{k^2e^2l\rho_{2DEG}}{m^*\epsilon_0\epsilon_r}}. \tag{4}$$

Several different metal-dielectric-2DEG configurations have been experimentally[32,33] and theoretically[34] studied, including stripe and disk gates[35,36] as well as lateral metallic gates,[37,38]

all generally leading to plasmonic dispersions interpolating between a linear and a square root dependence over the wavevector k. In our geometry, assuming the plasmon is localised in the defect of width w, it would be covered by gold except over the resonator gap of width d. We thus approximate the effective dielectric function with the weighted linear superposition

$$\bar{\epsilon}(k) = \frac{w-d}{w}\epsilon_{\mathrm{Au}}(k) + \frac{d}{w}\epsilon_{\mathrm{Air}}(k). \tag{5}$$

Doing so, and using the nominal parameters ($\epsilon_r = 13$, $\rho_{2DEG} = 3.2 \times 10^{11}$ cm^{-2}, $l = 90$ nm, $w = 1.5$ μm, $d = 250$ nm) leads to the first four plasmonic modes at frequencies 0, 336, 606, and 828 GHz. Taking into account that, as in the case of standard Bragg reflectors microcavities, the effective localization length would differ from the width of the defect w, and that exact modeling of the 90 nm etched sample simulations would require us to consider the residual coupling between the different plasmonic modes and the photonic resonator,[12] the agreement is good enough to allow us to identify the extra modes as higher lying plasmonic resonances of the plasmonic resonator.

Conclusion

Our recent paper demonstrated how Landau damping due to the continuum of propagating 2D plasmons can strongly modify the polaritonic spectrum of a device in which a 2DEG is coupled to a cSRR with sub-wavelength field confinement.[20] In this work we showed how the polaritonic features can be recovered by confining the plasmons using a plasmonic resonator. The proposed design is based on periodic one-dimensional structures on both sides of a central defect, to reflect the propagative magnetoplasmon waves and confine them close to the gap of the cSRR photonic resonator. Both theoretical and experimental results confirm we succeeded to confine the plasmons and we observed polaritonic resonances in a geometry in which they were not visible in the absence of the plasmonic reflectors. Still, as in our system the mode volume of the plasmonic resonator is substantially larger than the photonic

mode volume of the cSRR, the value of the normalized light-matter coupling, given by the overlap between the two, saturates and we could not substantially increase the strength of the light-matter coupling. We note that finite element simulations of a similar systems performed in Ref.,[12] in which the quantum well was laterally etched in a strip providing a perfect in-plane confinement to the plasmons, showed features which can be related to the experimental results presented in this paper. In such a simulation it is in-fact possible to see the plasmon localised not in the resonator gap but over the whole quantum well strip, while still being able to observe normal polaritonic resonances. Our result could be further improved by optimizing the reflector structure and can be extended to more general photonic resonator (e.g., direct SRR[6] or Bragg mirrors[9]), offering a generic solution to overcome the nonlocality-induced losses.

Acknowledgement

S.R., J.E., M.B., J.F., and G.S. acknowledge financial support from ERC Grant No. 340975-MUSiC and the Swiss National Science Foundation (SNF) through the National Centre of Competence in Research Quantum Science and Technology (NCCR QSIT).
S.D.L. acknowledges the support of a University Research Fellowship of the Royal Society and of the Phillip Leverhulme prize of the Leverhulme Trust. S.D.L. and E.C. acknowledge funding from the RPG-2022-037 grant of the Leverhulme Trust.

Data availability

Data underlying the results presented in this paper may be obtained from the authors upon reasonable request.

Disclosures

The authors declare no conflicts of interest.

References

(1) Jeannin, M.; Bonazzi, T.; Gacemi, D.; Vasanelli, A.; Li, L.; Davies, A. G.; Linfield, E.; Sirtori, C.; Todorov, Y. Absorption Engineering in an Ultrasubwavelength Quantum System. *Nano Lett.* **2020**, *20*, 4430–4436.

(2) Geiser, M.; Castellano, F.; Scalari, G.; Beck, M.; Nevou, L.; Faist, J. Ultrastrong Coupling Regime and Plasmon Polaritons in Parabolic Semiconductor Quantum Wells. *Phys. Rev. Lett.* **2012**, *108*, 106402.

(3) Forn-Díaz, P.; Lamata, L.; Rico, E.; Kono, J.; Solano, E. Ultrastrong coupling regimes of light-matter interaction. *Reviews of Modern Physics* **2019**, *91*.

(4) Frisk Kockum, A.; Miranowicz, A.; De Liberato, S.; Savasta, S.; Nori, F. Ultrastrong coupling between light and matter. *Nature Rev. Phys.* **2019**, *1*, 19–40.

(5) Hagenmüller, D.; De Liberato, S.; Ciuti, C. Ultrastrong coupling between a cavity resonator and the cyclotron transition of a two-dimensional electron gas in the case of an integer filling factor. *Phys. Rev. B* **2010**, *81*, 235303.

(6) Scalari, G.; Maissen, C.; Turčinková, D.; Hagenmüller, D.; De Liberato, S.; Ciuti, C.; Reichl, C.; Schuh, D.; Wegscheider, W.; Beck, M.; Faist, J. Ultrastrong Coupling of the Cyclotron Transition of a 2D Electron Gas to a THz Metamaterial. *Science* **2012**, *335*, 1323–1326.

(7) Bayer, A.; Pozimski, M.; Schambeck, S.; Schuh, D.; Huber, R.; Bougeard, D.; Lange, C. Terahertz Light-Matter Interaction beyond Unity Coupling Strength. *Nano Lett.* **2017**, *17*, 6340–6344.

(8) Li, X.; Bamba, M.; Zhang, Q.; Fallahi, S.; Gardner, G. C.; Gao, W.; Lou, M.; Yoshioka, K.; Manfra, M. J.; Kono, J. Vacuum Bloch–Siegert shift in Landau polaritons with ultra-high cooperativity. *Nature Photonics* **2018**, *12*, 324–329.

(9) Zhang, Q.; Lou, M.; Li, X.; Reno, J. L.; Pan, W.; Watson, J. D.; Manfra, M. J.; Kono, J. Collective non-perturbative coupling of 2D electrons with high-quality-factor terahertz cavity photons. *Nature Physics* **2016**, *12*, 1005–1011.

(10) Paravicini-Bagliani, G. L.; Appugliese, F.; Richter, E.; Valmorra, F.; Keller, J.; Beck, M.; Bartolo, N.; Rössler, C.; Ihn, T.; Ensslin, K.; Ciuti, C.; Scalari, G.; Faist, J. Magneto-transport controlled by Landau polariton states. *Nature Physics* **2018**, *15*, 186–190.

(11) Appugliese, F.; Enkner, J.; Paravicini-Bagliani, G. L.; Beck, M.; Reichl, C.; Wegscheider, W.; Scalari, G.; Ciuti, C.; Faist, J. Breakdown of topological protection by cavity vacuum fields in the integer quantum Hall effect. *Science* **2022**, *375*, 1030–1034.

(12) Cortese, E.; Mornhinweg, J.; Huber, R.; Lange, C.; De Liberato, S. Perspective on real-space nanophotonic field manipulation using non-perturbative light-matter coupling. *Optica* **2023**, *10*, 11.

(13) Rajabali, S.; Markmann, S.; Jöchl, E.; Beck, M.; Lehner, C. A.; Wegscheider, W.; Faist, J.; Scalari, G. An ultrastrongly coupled single terahertz meta-atom. *Nature Communications* **2022**, *13*, 2528.

(14) Keller, J.; Scalari, G.; Cibella, S.; Maissen, C.; Appugliese, F.; Giovine, E.; Leoni, R.; Beck, M.; Faist, J. Few-Electron ultrastrong light-matter coupling at 300 GHz with nanogap hybrid LC microcavities. *Nano letters* **2017**, *17*, 7410–7415.

(15) Ballarini, D.; De Liberato, S. Polaritonics: from microcavities to sub-wavelength confinement. *Nanophotonics* **2019**, *8*, 641–654.

(16) Ciracì, C.; Hill, R. T.; Mock, J. J.; Urzhumov, Y.; Fernández-Domínguez, A. I.; Maier, S. A.; Pendry, J. B.; Chilkoti, A.; Smith, D. R. Probing the Ultimate Limits of Plasmonic Enhancement. *Science* **2012**, *337*, 1072–1074.

(17) Gubbin, C. R.; De Liberato, S. Optical Nonlocality in Polar Dielectrics. *Phys. Rev. X* **2020**, *10*, 021027.

(18) Fernández-Domínguez, A. I.; Wiener, A.; García-Vidal, F. J.; Maier, S. A.; Pendry, J. B. Transformation-Optics Description of Nonlocal Effects in Plasmonic Nanostructures. *Phys. Rev. Lett.* **2012**, *108*, 106802.

(19) Gubbin, C. R.; De Liberato, S. Impact of phonon nonlocality on nanogap and nanolayer polar resonators. *Phys. Rev. B* **2020**, *102*, 201302.

(20) Rajabali, S.; Cortese, E.; Beck, M.; De Liberato, S.; Faist, J.; Scalari, G. Polaritonic nonlocality in light–matter interaction. *Nature Phot.* **2021**, *15*, 690–695.

(21) Cortese, E.; Carusotto, I.; Colombelli, R.; De Liberato, S. Strong coupling of ionizing transitions. *Optica* **2019**, *6*, 354–361.

(22) Cortese, E.; Tran, N.-L.; Manceau, J.-M.; Bousseksou, A.; Carusotto, I.; Biasiol, G.; Colombelli, R.; De Liberato, S. Excitons bound by photon exchange. *Nature Phys.* **2020**, 1–5.

(23) Cortese, E.; De Liberato, S. Exact solution of polaritonic systems with arbitrary light and matter frequency-dependent losses. *The Journal of Chemical Physics* **2022**, *156*, 084106.

(24) Qu, S.; Song, C.; Xia, X.; Liang, X.; Tang, B.; Hu, Z.-D.; Wang, J. Detuned plasmonic Bragg grating sensor based on a defect metal-insulator-metal waveguide. *Sensors* **2016**, *16*, 784.

(25) Song, C.; Xia, X.; Hu, Z.-D.; Liang, Y.; Wang, J. Characteristics of plasmonic Bragg reflectors with graphene-based silicon grating. *Nanoscale research lett.* **2016**, *11*, 1–8.

(26) Madeo, J.; Jukam, N.; Oustinov, D.; Rosticher, M.; Rungsawang, R.; Tignon, J.; Dhillon, S. S. Frequency tunable terahertz interdigitated photoconductive antennas. *Elec. Lett.* **2010**, *46*, 611–U25.

(27) Gallot, G.; Grischkowsky, D. Electro-optic detection of terahertz radiation. *J. Opt. Soc. Am. B* **1999**, *16*, 1204–1212.

(28) Scalari, G.; Maissen, C.; Cibella, S.; Leoni, R.; Reichl, C.; Wegscheider, W.; Beck, M.; Faist, J. THz ultrastrong light-matter coupling. *II Nuovo Saggiatore* **2015**, *31, 3-4*, 4–14.

(29) Hagenmüller, D.; De Liberato, S.; Ciuti, C. Ultrastrong coupling between a cavity resonator and the cyclotron transition of a two-dimensional electron gas in the case of an integer filling factor. *Phys. Rev. B* **2010**, *81*, 235303.

(30) Batke, E.; Heitmann, D.; Tu, C. Plasmon and magnetoplasmon excitation in two-dimensional electron space-charge layers on GaAs. *Physical Review B* **1986**, *34*, 6951.

(31) Chaplik, A. Absorption and emission of electromagnetic waves by two-dimensional plasmons. *Surface Science Reports* **1985**, *5*, 289–335.

(32) Huang, Y.; Qin, H.; Zhang, B.; Wu, J.; Zhou, G.; Jin, B. Excitation of terahertz plasmon-polariton in a grating coupled two-dimensional electron gas with a Fabry-Pérot cavity. *Applied Physics Letters* **2013**, *102*, 253106.

(33) Muravev, V.; Gusikhin, P.; Zarezin, A.; Andreev, I.; Gubarev, S.; Kukushkin, I. Two-dimensional plasmon induced by metal proximity. *Physical Review B* **2019**, *99*, 241406.

(34) Yoon, H.; Yeung, K. Y.; Kim, P.; Ham, D. Plasmonics with two-dimensional conductors. *Philosophical Transactions of the Royal Society A: Mathematical, Physical and Engineering Sciences* **2014**, *372*, 20130104.

(35) Zabolotnykh, A.; Volkov, V. Interaction of gated and ungated plasmons in two-dimensional electron systems. *Physical Review B* **2019**, *99*, 165304.

(36) Zabolotnykh, A.; Enaldiev, V.; Volkov, V. Quasistationary near-gate plasmons in van der Waals heterostructures. *Physical Review B* **2021**, *104*, 195435.

(37) Polischuk, O.; Popov, V.; Nikitov, S. Electromagnetic screening of plasmons in a two-dimensional electron system by lateral and topside gates. 2011 IEEE International Conference on Microwaves, Communications, Antennas and Electronic Systems (COMCAS 2011). 2011; pp 1–2.

(38) Popov, V. V.; Polishchuk, O.; Nikitov, S. A. Electromagnetic renormalization of the plasmon spectrum in a laterally screened two-dimensional electron system. *JETP letters* **2012**, *95*, 85–90.